Advanced Composites and Hybrid Materials (2022) 5:1888–1898
https://doi.org/10.1007/s42114-022-00508-0

ORIGINAL RESEARCH

Effective removal of proteins and polysaccharides from biotreated wastewater by polyaniline composites

Huiying Li[1] · Wen Huang[1] · Bin Qiu[1] · Hamdy Khamees Thabet[2] · Dalal Alhashmialameer[3] · Mina Huang[4,5] · Zhanhu Guo[5]

Received: 21 February 2022 / Revised: 7 May 2022 / Accepted: 24 May 2022 / Published online: 6 June 2022

Abstract

The proteins and polysaccharides are always remained in the effluent of biotreated process, which leads to further pollution for advanced treatment or aqueous environment. In this study, Fe_3O_4/polynailine composite (Fe_3O_4@PANI) was prepared by means of in situ surface polymerization, and was used as the adsorbent for removal of proteins and polysaccharides from biotreated wastewater. The removal rate of polysaccharide by PANI (69.43%) was higher than that by Fe_3O_4@PANI (61.33%), while the removal percentage of protein by Fe_3O_4@PANI (65.25%) was higher than that by original PANI (47.56%). The adsorption process was fitted well with the quasi-first-order kinetic and Langmuir isotherm models. Finally, it was determined that electrostatic attraction is the primary mechanism for the adsorption of proteins and polysaccharides by PANI-based materials.

Keywords Protein · Polysaccharide · Polyaniline · Fe_3O_4@PANI composite · Adsorption

1 Introduction

Recently, the domestic wastewater is usually treated by biological technologies, including aerobic and anaerobic methods [1]. Compared with aerobic biological treatment, the anaerobic treatment is feasible for sewage treatment due to its easy resource recovery and low operation costs [2]. Nowadays, anaerobic membrane bioreactor (AnMBR), which combines membrane separation and anaerobic biological treatment, has been attracted increasing attention for sewage treatment. However, the membrane fouling is considered as one of the challenges for the operation of AnMBR. As was known, large number of organics were remained in the effluent of anaerobic treatment unit, including residual biodegradable and non-biodegradable substrates, intermediate products, and complex dissolved microbial products (SMP) [3]. In addition, the soluble extracellular polymeric substances (EPS) secreted by microorganisms were also remained in the biotreated wastewater [4].

The SMP and soluble EPS remained in the biotreated wastewater can easily cause the disinfection by-products, which would lead to the risk on the environmental and human health [5]. It was the bacterial clusters would form the filter cake layer on the surface of membrane, which leads to the membrane fouling. Besides, the biopolymers, organic matters, and inorganic matters were also found as the main pollutants in the filter cake layer [6]. Nowadays, the control of biological fouling has attracted widespread concern for the membrane separation operation [7–9]. Also, the SMP and EPS also play an important role in the formation of filter

✉ Bin Qiu
qiubin2015@bjfu.edu.cn

✉ Hamdy Khamees Thabet
hamdy.salem@nbu.edu.sa

✉ Zhanhu Guo
zguo10@utk.edu

[1] Beijing Key Laboratory for Source Control Technology of Water Pollution, College of Environmental Science and Engineering, Beijing Forestry University, Beijing 100083, China

[2] Chemistry Department, Faculty of Arts and Science, Northern Border University, PO 840, Rafha 91911, Saudi Arabia

[3] Department of Chemistry, College of Science, Taif University, Taif 21944, Saudi Arabia

[4] College of Materials Science and Engineering, Taiyuan University of Science and Technology, Taiyuan 030024, China

[5] Integrated Composites Laboratory (ICL), Department of Chemical and Biomolecular Engineering, University of Tennessee, 1512 Middle Dr, Knoxville, TN 37996, USA

cake layer, causing severe membrane fouling [9, 10]. Thus the mitigation of biological membrane fouling was the one of the main challenges for the application of AnMBR [11]. The proteins (PN) and polysaccharides (PS) are the main components of EPS, and they account for more than 70% of the total mass of EPS [8]. Therefore, removal of the PN and PS in the biotreated wastewater seems to be important for mitigating the membrane fouling for the AnMBR.

Various techniques were used to remove the dissolved organic matters in wastewater, including the flocculation, oxidation, and adsorption [12, 13]. Among these methods, the adsorption was commonly used due to its easy operation and low cost [13]. Recently, the activated carbon materials have been widely used to adsorb the EPS in the wastewater [14–16]. Besides, the polyaniline (PANI), as a typical conductive polymer, has been widely used in various applications, such as coatings, batteries, absorbing materials, sensors, and conductive fibers [17–22]. In anaerobic digestion systems, it is also used as a conductive material to improve extracellular electron transfer efficiency and promote methane production [23]. Aboundant amine and imine groups are contained on the PANI chains, and the imine groups are easily doped with protons. The positive charge carried by the proton can be transferred in the molecular chain, which leads to positively charged surface of PANI [24]. As was known, the proteins and polysaccharides are often negatively charged in the wastewater [20]. PANI is supposed to be effective on adsorption removal of the negatively charged proteins and polysaccharides as it is always positively charged in the neutral solution. However, the adsorption performance of PN and PS from the biotreated wastewater by the conductive PANI has not been reported.

In this study, conductive PANI and core–shell structured Fe_3O_4@PANI composites with a high electric point were prepared which served as the adsorbent for removing the remained PN and PS from the biotreated wastewater. The adsorption performance of PANI and Fe_3O_4@PANI composites on the PN and PS was investigated as well as the adsorption kinetics and isotherms. Finally, the removal mechanisms were also disclosed.

2 Experimental section

2.1 Materials

Aniline, ammonium persulfate, hydrochloric acid, nano-ferric oxide, glucose, bovine serum albumin, sodium carbonate, sodium potassium tartrate tetrahydrate, sodium hydroxide, folin phenol, anthrone, and sulfuric acid were provided by Beijing Chemical Works, China. None of the chemicals had undergone any purification.

2.2 Preparation of PANI and Fe_3O_4@PANI

Preparation of PANI by chemical oxidative polymerization [23, 25, 26] Briefly, 3.2 mL of aniline and 8.22 g of ammonium persulfate were added in to 100 mL of HCl solution (54 mmol/L), respectively. The prepar The mixed solution was stirred at 600 rpm below 0 °C for 4 h until a dark green solid formed in the reaction system. Subsequently, the solid samples were separated by suction filtration separation, and then suction filtration washing with acetone or alcohol and deionized water until the filtrate becomes colorless. The obtained solids were vacuum-dried at 60 °C for 12 h to obtain the PANI sample.

The Fe_3O_4@PANI was prepared by an in situ surface polymerization method [27, 28]. Briefly, 0.6 g of nano-scaled Fe_3O_4 was added into 200 mL of HCl solution (54 mmol/L), and the mixed solution was mechanically stirred for 15 min. Then 3.2-mL aniline monomer was added, and further stirred for 30 min to well disperse them in the solution. Then 100 mL of APS solution was put in the aniline solution dropwise. The mixture was stirred at 600 rpm in the ice bath until a dark black solid formed in the reaction system. Subsequently, the solid sample was separated from the reaction system by suction filtration, and then suction filtration washing with acetone or alcohol and deionized water until the filtrate becomes colorless. The obtained solids were vacuum-dried at 60 °C for 12 h to obtain the Fe_3O_4@PANI sample.

2.3 Protein and polysaccharide adsorption

The artificial wastewater was prepared and used to the adsorption tests in this study. A mixture solution with 40 mg/L of PN and 25 mg/L of PS was prepared as the storage solution. One-hundred milliliters of the mixture solution was added into the beakers, and then the desired dosage (0.2 g/L) of PANI or Fe_3O_4@PANI composites were added, respectively. The adsorption reaction was carried out in a shaker with a speed of 300 rpm for 12 h. Before measuring the concentration of the PN and PS, the solution was collected and filtrated by 0.45-μm filter. For the kinetic investigation, the same procedures were conducted as motioned above. PANI or Fe_3O_4@PANI adsorbents were added into the prepared solutions, and then the adsorption was carried out at 35 °C with stirring at 100 rpm. The water samples were collected at different time intervals. For isotherm experiments, the PN and PS solutions with different initial concentrations were prepared. Then 50 mg PANI or Fe_3O_4@PANI adsorbents were added to the solutions, and adsorption experiments were carried out at 25 °C and 35 °C, respectively. The concentration of PN remained in the

solutions was detected by the Folin-Lowry method using the bovine serum albumin as the standard [29], and the concentration of PS was determined by the anthrone-sulfuric acid method using the glucose as the standard [30].

2.4 Characterizations

The morphology of the PANI and Fe_3O_4@PANI composite was detected by a JSM-F100 scanning electron microscope. The Fe_3O_4@PANI structure was detected by a transmission electron microscope (Tecnai G2 F20, FEI). The functional groups of the synthesized materials were determined by FT-IR (ALPHA, Bruker). An X-ray photoelectron spectrometer (AXIS Ultra DLD, Shimadzu) was used to determine the valence states of the elements in PANI and Fe_3O_4@PANI materials. The zeta potential of the materials was detected by a zeta potentiometer (Nano Z, Marvin). Fluorescence spectrometer (F-7000, Hitachi) was used for detecting the proteins remained in the solutions.

3 Results and discussion

3.1 Characterizations

As shown in Fig. S1, the pristine PANI has a regular nanorod-like structure with an average length of about 3 μm and a diameter of ~ 100 nm. Besides, the PANI material has a rough surface, which might provide abundant active sites for adsorption of organic pollutants in the wastewater. As shown in Fig. 1a, the synthesized Fe_3O_4@PANI composite has an irregular spherical morphology with a rough surface. The average diameter of Fe_3O_4@PANI particle is determined as ~ 200 nm. Figure 1b further reveals the regular spherical structure of Fe_3O_4@PANI composite. The Fe_3O_4 particles used in this study are about 100 nm in diameter, and PANI is obviously coated around the Fe_3O_4 particles, forming the core–shell structured Fe_3O_4@PANI. The magnetic Fe_3O_4 core leads to the easy separation of the composites after being used from the wastewater.

The valence state of N element in pristine PANI and Fe_3O_4@PANI composite was analyzed by XPS (Fig. 2). The binding energy peaks at 399.3, 400.4, and 402.0 eV correspond to the –N = group in the quinone ring, – NH – group in the benzene ring and the proton doping N^+ groups [28, 31, 32], respectively. There is no obvious difference between the spectra of PANI and Fe_3O_4@PANI, indicating that Fe_3O_4 has no obvious effect on the state of PANI. The equal intensities of – N = and – NH – in the N1s XPS spectra indicate that PANI exists in the form of emeralds [33]. Moreover, proton doping leads to positively charged surface of PANI, which facilitates adsorption of the negatively charged biomacromolecules. Figure 2c shows the FTIR spectra of original polyaniline and Fe_3O_4@PANI. The characteristic peaks located at 1490 and 1568 cm^{-1} correspond to the C = C stretching vibration of benzene ring and quinone ring of PANI [34, 35]. The characteristic absorption peak at 1290 cm^{-1} is the stretching vibration of C–N in aromatic amine, and the peak at 1033 cm^{-1} is the in-plane bending vibration of C–H caused by protonation [36–38]. The characteristic absorption peak at 794 cm^{-1} is C–H out-of-plane bending vibration [39]. It was found that all the characteristic peaks of the PANI also appeared in the spectra of Fe_3O_4@PANI, and no obvious difference was detected between the PANI and Fe_3O_4@PANI. This result was consistent with the XPS (Fig. 2a, b). However, the characteristic peak of bending vibration in the C–H plane was blue-shifted, indicating the interaction of the PANI and Fe_3O_4 during the polymerization process [40, 41]. A new peak was also found in the spectrum of Fe_3O_4@PANI, at 556 cm^{-1}, which was owing to the vibration of Fe–O [42]. It indicated that the Fe_3O_4 was successfully coated with PANI.

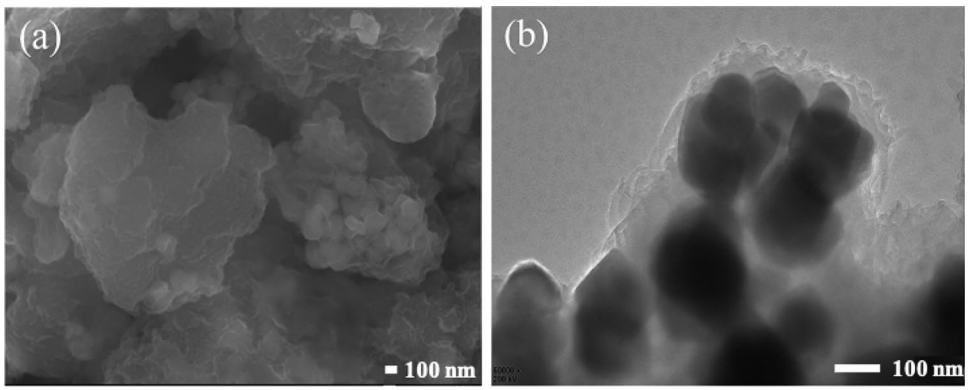

Fig. 1 (**a**) SEM and (**b**) TEM images of Fe_3O_4@PANI composite

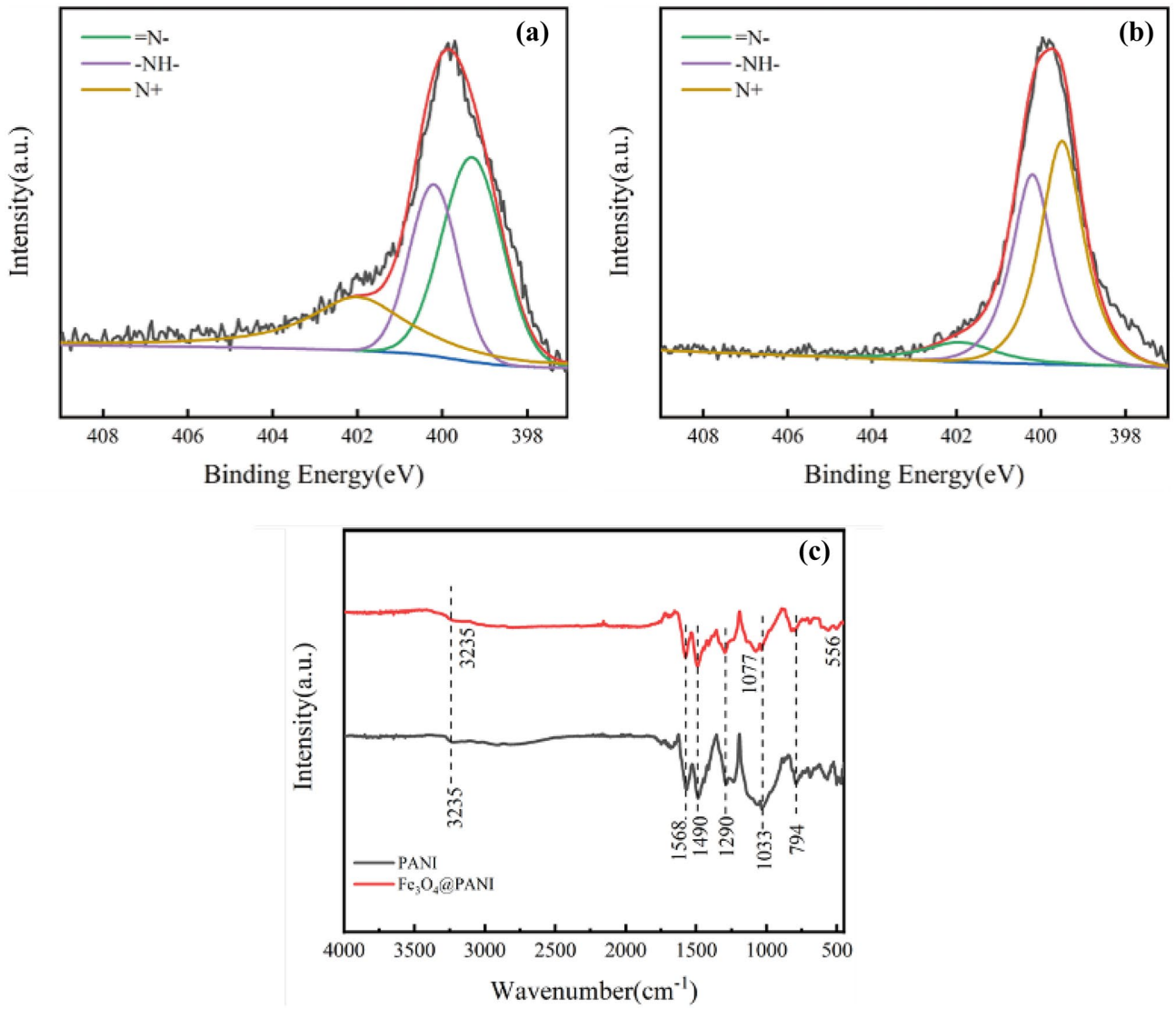

Fig. 2 N1s XPS spectra of (**a**) PANI and (**b**) Fe_3O_4@PANI composite and (**c**) FT-IR spectra of PANI and Fe_3O_4@PANI composite

3.2 Adsorption performance

3.2.1 Adsorption removal rate

The removal performance of the PANI composites on the PN and PS was investigated. The pristine PANI and Fe_3O_4@PANI materials can effectively remove PN and PS. As shown in Fig. 3, 47.56% of PN was removed by the pristine PANI material when 0.2 g/L of the adsorbents was added. Moreover, 65.25% of PN was adsorbed by the Fe_3O_4@PANI composite, which is higher than the pristine PANI. About 69.43% of PS was removed from the wastewater by 0.2 g/L of pristine PANI, which is a little higher than that by the Fe_3O_4@PANI composites (61.33%). It was inferred that pristine PANI has a better performance on adsorption removal of PS than Fe_3O_4@PANI composite, while Fe_3O_4@PANI performed better on PN removal than pristine PANI. As was known, the positive charged surface of PANI can adsorb the negatively charged PN and PS by the electrostatic attraction. Besides, the Fe_3O_4 also provides the active sites for PN adsorption. Thus Fe_3O_4 and PANI was inferred to have the synergistic effect for removing PN. However, magnetic Fe_3O_4 could make the Fe_3O_4@PANI composites agglomerate easily in the wastewater [43], reducing the active sites on the surface of PANI for PS adsorption, which decreased the PS adsorption performance of Fe_3O_4@PANI.

As was documented, the chitosan was commonly used for adsorption of proteins and polysaccharides from the

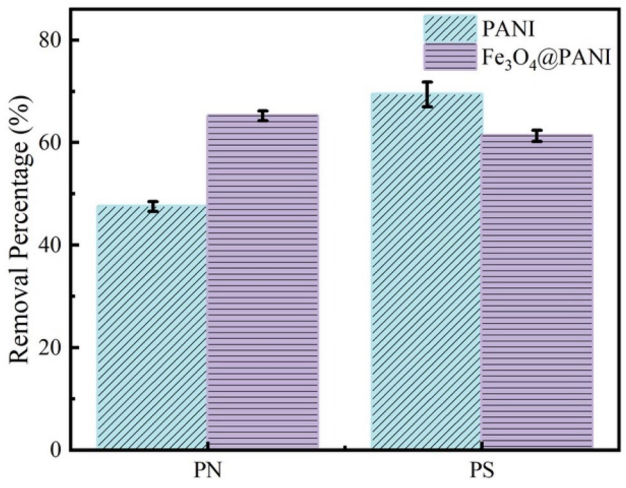

Fig. 3 Adsorption removal of PN and PS by pristine PANI and Fe_3O_4@PANI composite

aqueous solution [44, 45]. For example, 45% and 60% of proteins can be removed by chitosan when the adsorbent dosage was controlled at 1 g/L and 10 g/L [46]. This indicated that PANI-based materials have the similar adsorption performance, but 0.2 g/L of the adsorbents dosage was much lower than chitosan. Meanwhile, macro-porous resins were commonly used for removing the polysaccharides from aqueous solution [47, 48]. Sixty-six percent of polysaccharides can be removed by 10 g/L of macro-porous resin [49, 50]. For achieving the same adsorption performance, the dosage of PANI-based materials used in this study was much lower than that of macro-porous resin.

3.2.2 Adsorption kinetics

The removal process of PN and PS process from the wastewater by the pristine PANI and Fe_3O_4@PANI composite was fitted by using the adsorption kinetic models [51]. The information of the models is presented in the Supporting materials, and fitting results are listed in Table S1. As shown in Figs. 4 and S3, the correlation coefficient (R^2) fitted by the first-order kinetic model is significantly higher than that by the second-order kinetic model. Moreover, the equilibrium adsorption capacity calculated by the first-order kinetic model is closer to the experimental value. It indicates that PN and PS removal processes by both the pristine PANI and Fe_3O_4@PANI fit well with first-order kinetic, and the Fe_3O_4 has no obvious effect on the adsorption of PN and PS by the PANI. It can be inferred that the PN and PS removal by both the pristine PANI and Fe_3O_4@PANI is based on the boundary diffusion, and these adsorption processes are controlled by the physical adsorption. The adsorption process depends in part on the number of surface active adsorption sites of the adsorbent [52].

3.2.3 Adsorption isotherms

The Langmuir and Freundlich isotherm models were used to simulate the adsorption processes of PN by both the pristine PANI and Fe_3O_4@PANI (Fig. 5). The information of the isotherm models is presented in the Supporting materials, and fitting results are listed in Table S2. Table S2 shows that the correlation coefficient (R^2) fitting with the Langmuir model is significantly higher than that with the Freundlich model. Therefore, the Langmuir model can better describe the

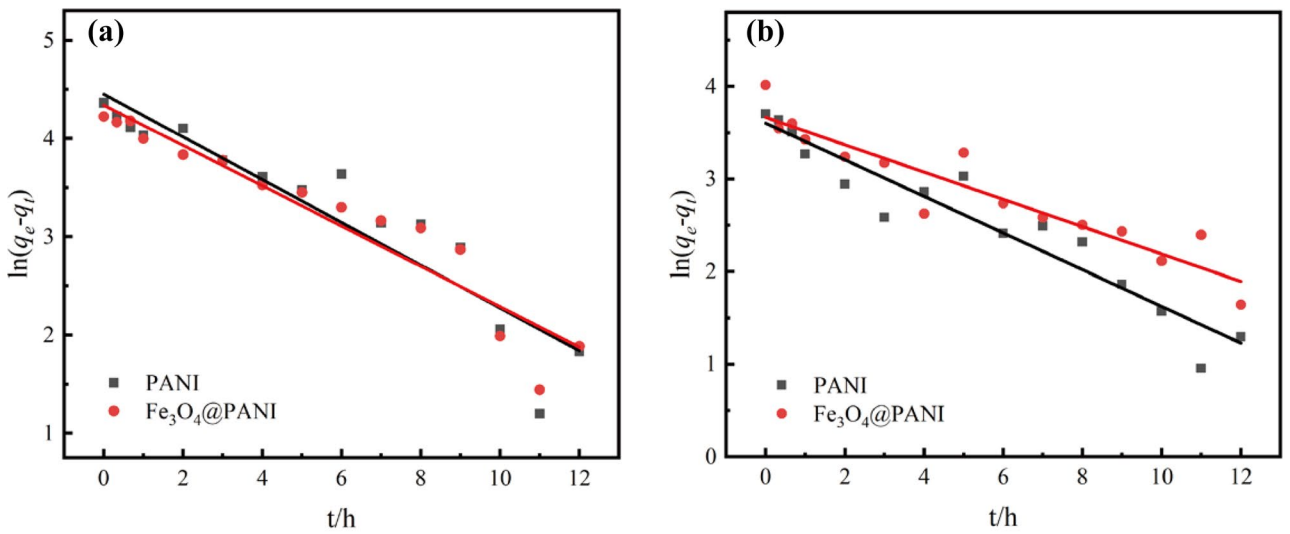

Fig. 4 First-order kinetic model for adsorption of (**a**) PN and (**b**) PS by PANI and Fe_3O_4@PANI

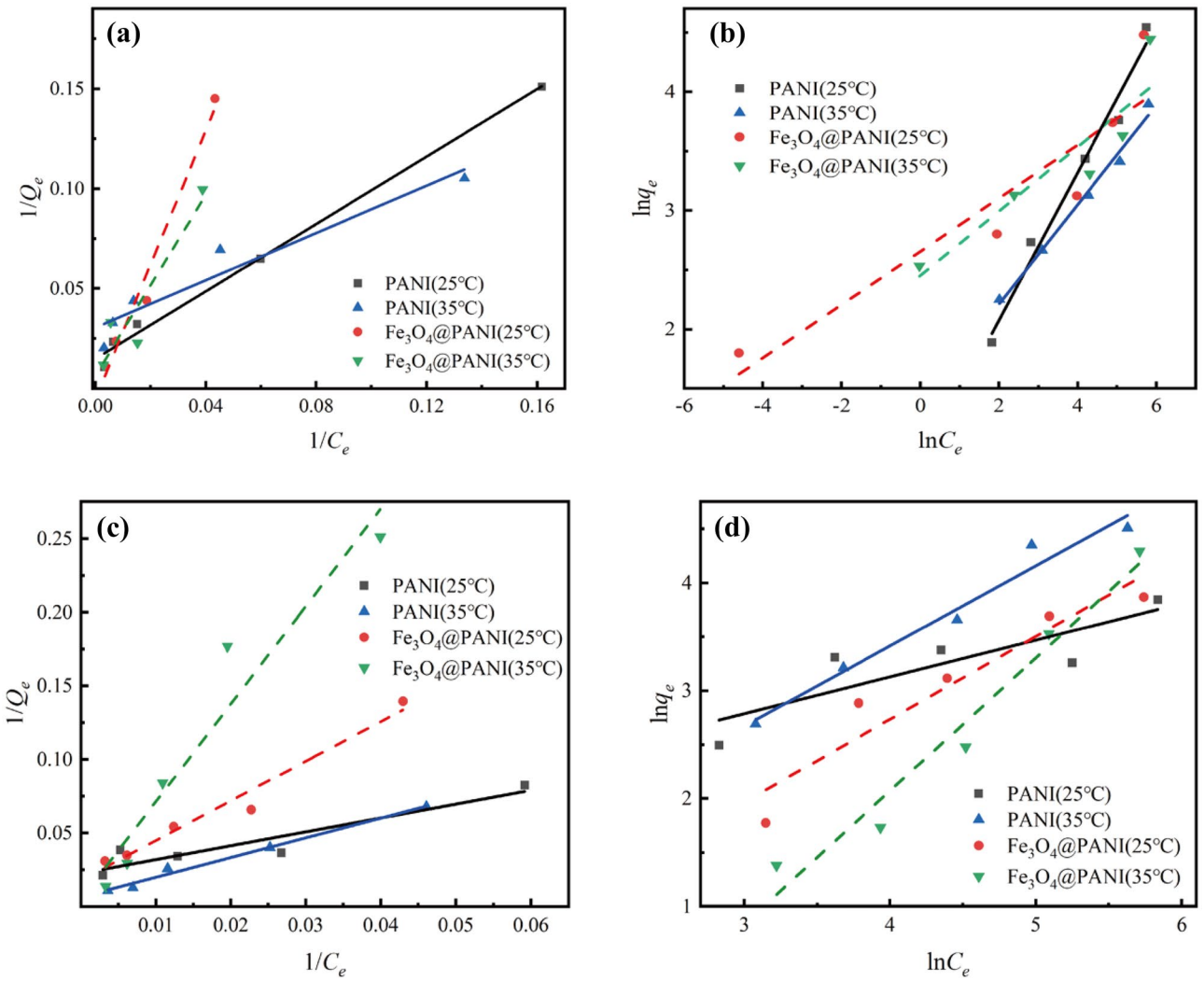

Fig. 5 PN absorption fitting with (**a**) Langmuir and (**b**) Freundlich isotherm and PS absorption fitting with (**c**) Langmuir and (**d**) Freundlich isotherm

adsorption behavior of PN by the PANI and Fe_3O_4@PANI. This also indicates that the removal of PN by the PANI and Fe_3O_4@PANI is a single molecule layer adsorption, and the PN substances would occupy adsorption sites on the surface of the PANI and Fe_3O_4@PANI adsorbents [53, 54]. The maximum PN adsorption capacity of Fe_3O_4@PANI is calculated as 104.65 mg/g, which is much higher than 87.30 mg/g of PANI (Table S2).

Figure 5c, d show that the correlation coefficient (R^2) fitting with the Langmuir model is significantly higher than that with the Freundlich model, indicating that the Langmuir model fits better with the PS adsorption process by both the pristine PANI and Fe_3O_4@PANI. This indicates that the PS removal is a monolayer adsorption process, which is similar with the PS removal process. The maximum PS adsorption capacity of Fe_3O_4@PANI is calculated as 196.85 mg/g with the reaction temperature at 35 °C, which is much higher than 152.91 mg/g of PANI (Table S2).

3.3 Adsorption mechanism

3.3.1 3D fluorescence spectrum

The adsorption characteristics of fluorescent substances in wastewater were characterized by three-dimensional fluorescence spectroscopy (EEM) (Fig. 6). Two characteristic peaks were detected in the spectra of the wastewater, and the peaks at $E_x/E_m = 222/344$ nm and $E_x/E_m = 275/342$ nm are related the aromatic and tryptophan protein substances [55]. The results show that the peak intensity decreases with the increase of adsorption time, and the weak intensity of both the two peaks was observed after 24 h of adsorption by

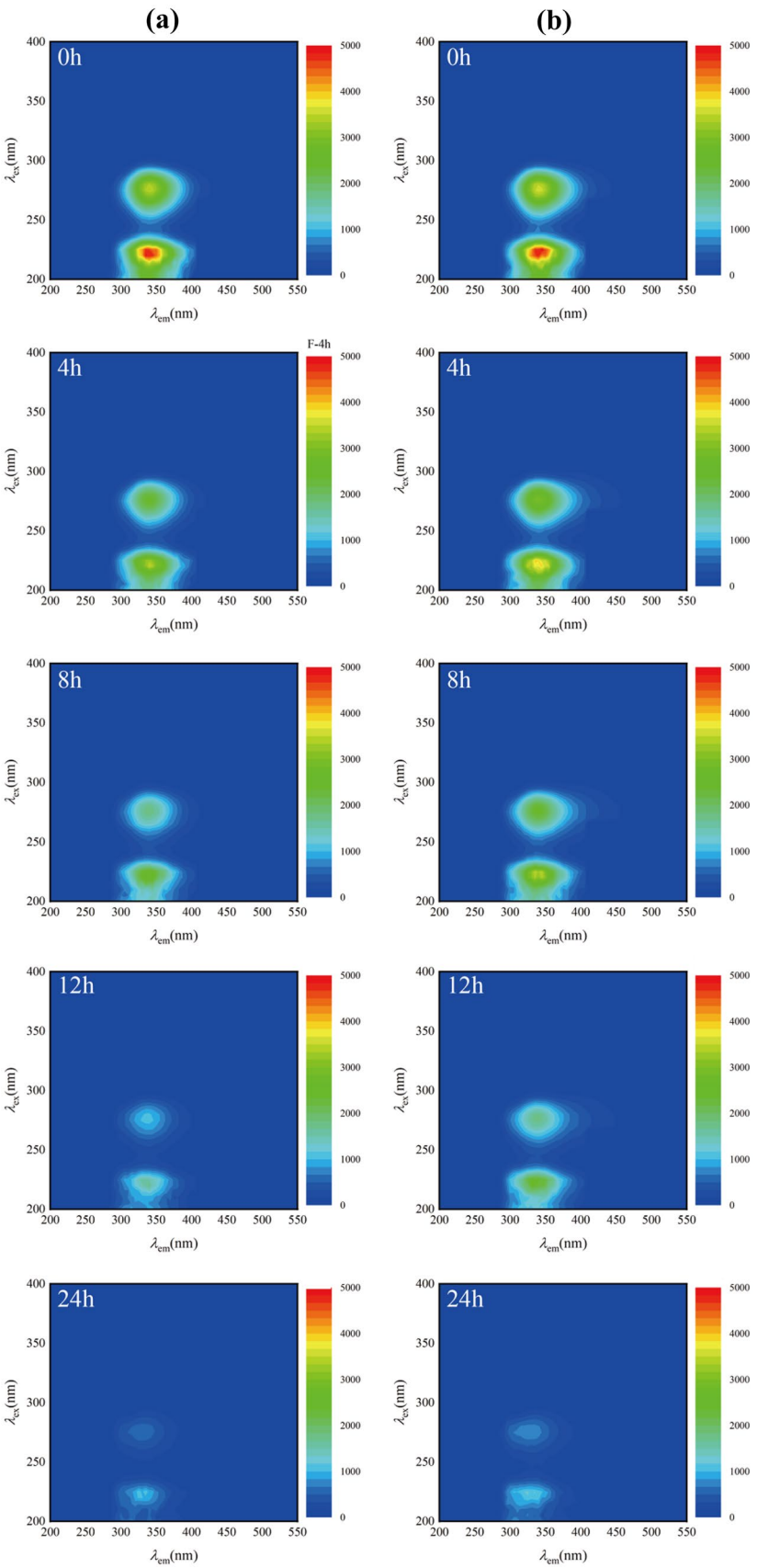

Fig. 6 3D-EEM images of the wastewater treated by the (**a**) Fe_3O_4@PANI and (**b**) pristine PANI

both the PANI and Fe_3O_4@PANI, indicating the good performance of the PANI-based materials on the removal of PN substances. It was also found that the peaks intensity of the wastewater treated by the Fe_3O_4@PANI was lower than that by the pristine PANI, which suggests that Fe_3O_4@PANI has a better performance on removal of proteins than PANI. This is consistent with the result of the adsorption experiment.

3.3.2 SEM–EDS and TEM

Figure 7 shows the SEM and TEM images of the Fe_3O_4@PANI after treatment of the wastewater. Fe_3O_4@PANI presents as the obvious particles, and the particles were surrounded with a loosen layer of substances. It was inferred that the proteins and polysaccharides were adsorbed and formed a rough surface of the Fe_3O_4@PANI. Moreover, the obvious core–shell structure of the Fe_3O_4@PANI was also observed after the treatment of wastewater. No obvious change was observed for the materials before and after being used, which indicated that the Fe_3O_4@PANI has good stability for treating this wastewater.

Figure S4 shows the composition of elements in the Fe_3O_4@PANI and PANI before and after treating the wastewater, and the elemental contents were listed in Table S4. Of the C, 72.49% and of N, 17.10% were detected for PANI after adsorption, which was obviously higher than these in the pristine PANI. However, the percentage of O in PANI decreased. For the Fe_3O_4@PANI, only the percentage of N element increased to 18.34% after adsorption, while the percentage of C and O decreased. It was inferred that the PANI-based materials were preferred to adsorption of PN. The PN contains abundant N; thus, the high adsorption capacity led to the increase of the N element on the surface of the adsorbents. The higher increase of N element in Fe_3O_4@PANI composite indicated the Fe_3O_4@PANI has a better performance on PN adsorption than pristine PANI. The percentage of Fe in the composite also significantly decreased. The adsorbed PN and PS formed a layer surrounding the composite, which weakened the intensity of Fe.

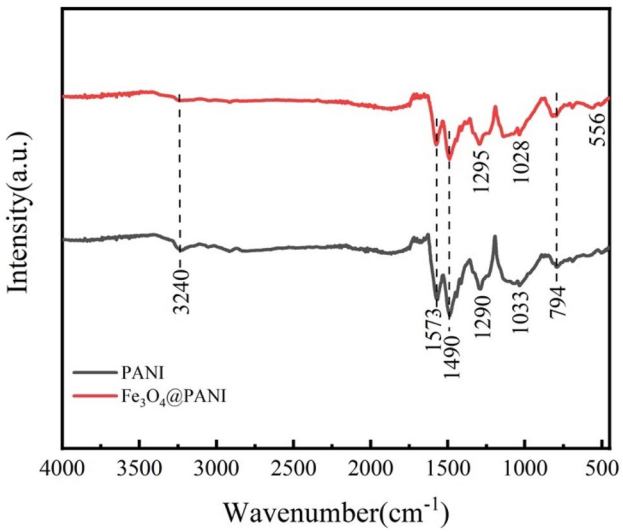

Fig. 8 FT-IR spectra of PANI and Fe_3O_4@PANI after treating the wastewater

3.3.3 FTIR characterization

FT-IR spectra of PANI-based materials after wastewater treatment are shown in Fig. 8. Compared with the synthesized PANI and Fe_3O_4@PANI (Fig. 2c), the characteristic peaks of the C = C stretching vibration of the quinone ring on polyaniline undergo a slight blue shift after adsorption, which inferred that the imine groups (−N=) are the main active sites for the PN and PS adsorption. For Fe_3O_4@PANI, a little shift was also observed at the characteristic peaks of 1568 and 1290 cm^{-1}, which also indicates indicating that PN and PS are adsorbed on the imine groups (−N=) of the composite.

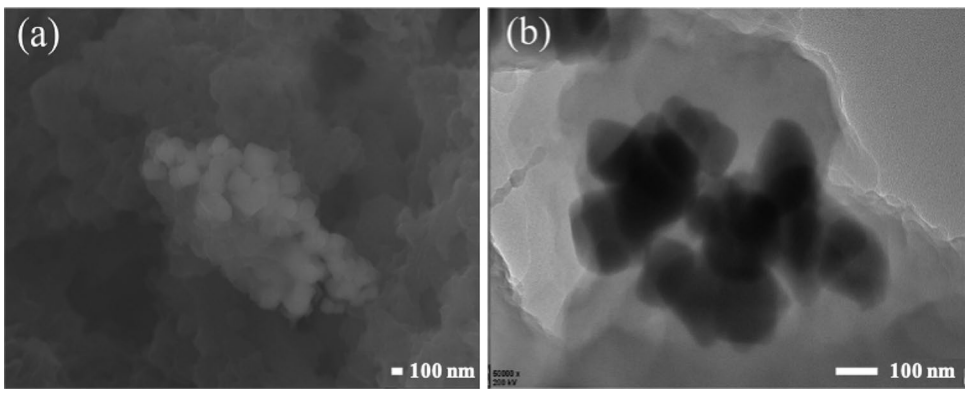

Fig. 7 (**a**) SEM and (**b**) TEM images of Fe_3O_4@PANI after treatment of wastewater

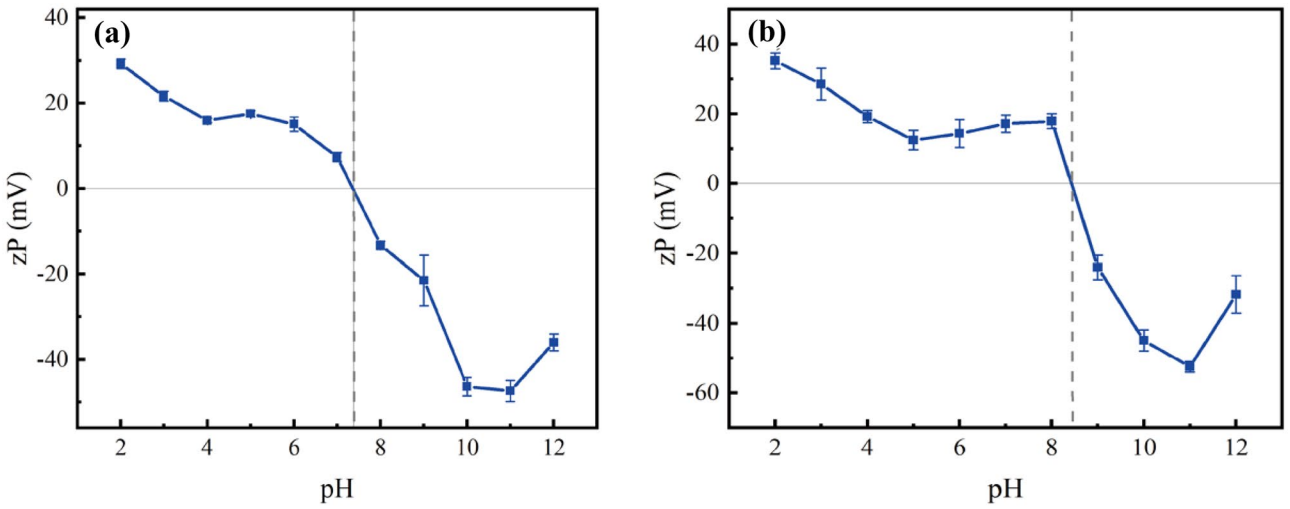

Fig. 9 Zeta potential of (**a**) PANI and (**b**) Fe_3O_4@PANI

3.3.4 Zeta potential

The measurement results of zeta potential of Fe_3O_4@PANI and PANI adsorbents are shown in Fig. 9. Figure 9a shows that the isoelectric point (P_i) of PANI is about pH at 7.3, which indicates that the PANI surface is positively charged when pH is lower than 7.3. The high P_i is due to the dopped protons in the imine groups in the PANI chains. Besides, the P_i of Fe_3O_4@PANI increases to pH at 8.4. The P_i of proteins and polysaccharides was detected as pH at 4.9 and 2.5 (Fig. S5), respectively. It was inferred that proteins existed as negatively charged amino acid ions when the aqueous pH is above 4.9, and polysaccharides also exist as negatively charged amino acid when aqueous pH is above 2.5. Thus, the positively charged adsorbents can easily adsorb the negatively charged proteins and polysaccharides in the wastewater by the electrostatic attraction.

4 Conclusion

The PANI and core–shell structured Fe_3O_4@PANI composites were synthesized and were demonstrated as the alternative adsorbents for further removal of the PN and PS from the biotreated wastewater. The adsorption of proteins and polysaccharides by both the PANI and Fe_3O_4@PANI were fitted well with the first-order kinetic and Langmuir isotherm models. The adsorption capacity of Fe_3O_4@PANI for PN was 104.65 mg/g, which was much higher than pristine PANI (87.30 mg/g). While adsorption capacity of PANI for PS was 196.85 mg/g, which was higher than Fe_3O_4@PANI (152.91 mg/g). The electrostatic attraction was determined as the main mechanism involved in the adsorption of PN and PS by the PANI and Fe_3O_4@PANI.

Supplementary information The online version contains supplementary material available at https://doi.org/10.1007/s42114-022-00508-0.

Funding This work is supported by the Fundamental Research Funds for the Central Universities (2021ZY77). The authors also extend their appreciation to the Deputyship for Research & Innovation, Ministry of Education in Saudi Arabia for funding this research work through the project number "x_2020_IF."

Declarations

Conflict of interest The authors declare no competing interests.

References

1. Wainaina S et al (2020) Resource recovery and circular economy from organic solid waste using aerobic and anaerobic digestion technologies. Bioresour Technol 301:122778. https://doi.org/10.1016/j.biortech.2020.122778
2. Li LL, Tong ZH, Fang CY, Chu J, Yu HQ (2015) Response of anaerobic granular sludge to single-wall carbon nanotube exposure. Water Res 70:1–8. https://doi.org/10.1016/j.watres.2014.11.042
3. Benyahia B, Sari T, Harmand J, Cherki B (2011) Modeling of the soluble microbial products (SMP) in anaerobic membrane bioreactors (AMBR): equilibria and stability of the AM2b model. IFAC Proc 44:3789–3794. https://doi.org/10.3182/20110828-6-IT-1002.01195
4. Lee DY, Li YY, Noike T, Cha GC (2008) Behavior of extracellular polymers and bio-fouling during hydrogen fermentation with a membrane bioreactor. J Membr Sci 322:13–18. https://doi.org/10.1016/j.memsci.2008.04.031
5. Wu M, Liang Y, Peng H, Ye J, Wu J, Shi W, Liu W (2019) Bioavailability of soluble microbial products as the autochthonous precursors of disinfection by-products in aerobic and anoxic surface water. Sci Total Environ 649:960–968. https://doi.org/10.1016/j.scitotenv.2018.08.354
6. Wisniewski C, Grasmick A (1998) Floc size distribution in a membrane bioreactor and consequences for membrane fouling.

Colloid Surface A 138:403–411. https://doi.org/10.1016/S0927-7757(96)03898-8
7. Sunny W, Greg G, Hoek Eric MV (2005) Direct observation of microbial adhesion to membranes. Environ Sci Technol 39:6461–6469. https://doi.org/10.1021/es050188s
8. Meng PC, Peiying H, Huiling G, Wen TL (2005) Biofilm formation characteristics of bacterial isolates retrieved from a reverse osmosis membrane. Environ Sci Technol 39:7541–7550. https://doi.org/10.1021/es050170h
9. Chen MY, Lee DJ, Tay J (2006) Extracellular polymeric substances in fouling layer. Sep Sci Technol 41:1467–1474. https://doi.org/10.1080/01496390600683597
10. Ramesh A, Lee D, Wang M, Hsu J, Juang R, Hwang K, Liu J, Tseng S (2006) Biofouling in membrane bioreactor. Sep Sci Technol 41:1345–1370. https://doi.org/10.1080/01496390600633782
11. Visvanathan C, Abeynayaka A (2012) Developments and future potentials of anaerobic membrane bioreactors (AnMBRs). Membr Water Treat 3:1–23. https://doi.org/10.12989/mwt.2012.3.1.001
12. Zhang W, Cao B, Wang D, Ma T, Xia H, Yu D (2016) Influence of wastewater sludge treatment using combined peroxyacetic acid oxidation and inorganic coagulants re-flocculation on characteristics of extracellular polymeric substances (EPS). Water Res 88:728–739. https://doi.org/10.1016/j.watres.2015.10.049
13. Davis JA (1982) Adsorption of natural dissolved organic matter at the oxide/water interface. Geochim Cosmochim Acta 46:2381–2393. https://doi.org/10.1016/0016-7037(82)90209-5
14. Kim J, Kim K, Ye H, Lee E, Shin C, McCarty PL, Bae J (2011) Anaerobic fluidized bed membrane bioreactor for wastewater treatment. Environ Sci Technol 45:576–581. https://doi.org/10.1021/es1027103
15. Chen L, Cheng P, Ye L, Chen H, Xu X, Zhu L (2020) Biological performance and fouling mitigation in the biochar-amended anaerobic membrane bioreactor (AnMBR) treating pharmaceutical wastewater. Bioresource Technol 302:122805. https://doi.org/10.1016/j.biortech.2020.122805
16. Luo X, Yang G, Schubert DW (2021) Electrically conductive polymer composite containing hybrid graphene nanoplatelets and carbon nanotubes: synergistic effect and tunable conductivity anisotropy. Adv Compos Hybrid Ma. https://doi.org/10.1007/s42114-021-00332-y
17. Nguyen TD, Nguyen TA, Pham M, Piro B, Normand B, Takenouti H (2004) Mechanism for protection of iron corrosion by an intrinsically electronic conducting polymer. J Electroanal Chem 572:225–234. https://doi.org/10.1016/j.jelechem.2003.09.028
18. Bleda-Martínez MJ, Morallon E, Cazorla-Amorós D (2007) Polyaniline/porous carbon electrodes by chemical polymerisation: effect of carbon surface chemistry. Electrochim Acta 52:4962–4968. https://doi.org/10.1016/j.electacta.2007.01.073
19. Humpolíček P et al (2015) Stem cell differentiation on conducting polyaniline. RSC Adv 5:68796–68805. https://doi.org/10.1039/C5RA12218J
20. Lü Z, Xiujuan X, Biao P, Guofeng F (2016) Extracellular polymeric substance (EPS) characteristics and comparison of suspended and attached activated sludge at low temperatures. J Thu (Sci Technol) 56:1009–1015. https://doi.org/10.16511/j.cnki.qhdxxb.2016.21.051
21. Zhang F, Cui W, Wang B, Xu B, Liu X, Liu X, Jia Z, Wu G (2021) Morphology-control synthesis of polyaniline decorative porous carbon with remarkable electromagnetic wave absorption capabilities. Compos Part B-Eng 204:108491. https://doi.org/10.1016/j.compositesb.2020.108491
22. Ingle R V, Shaikh S F, Bhujbal P K, Pathan H M, Tabhane VA (2020) Polyaniline doped with protonic acids: optical and morphological studies. ES Mater Mfg 8:54–59. https://doi.org/10.30919/esmm5f732
23. Hu Q, Zhou J, Qiu B, Wang Q, Song G, Guo Z (2021) Synergistically improved methane production from anaerobic wastewater treatment by iron/polyaniline composite. Adv Compos Hybrid Ma 2:265–273. https://doi.org/10.1021/acssuschemeng.8b05847
24. Liu S, Liu X, Li Z, Yang S, Wang J (2011) Fabrication of free-standing graphene/polyaniline nanofibers composite paper via electrostatic adsorption for electrochemical supercapacitors. New J Chem 35:369–374. https://doi.org/10.1039/C0NJ00718H
25. Liao Y, Wang Y, Ouyang L, Dong Y, Zhou J, Hu Q, Qiu B (2021) Conductive polyaniline enhanced decolorization of azo dyes in anaerobic wastewater treatment. FAF 6: 35–42. https://doi.org/10.30919/esfaf584
26. Li S et al (2019) Facile synthesis of nanostructured polyaniline in ionic liquids for high solubility and enhanced electrochemical properties. Adv Compos Hybrid Ma 2:279–288. https://doi.org/10.1007/s42114-019-00103-w
27. Guo J, Chen Z, Abdul W, Kong J, Khan MA, Young DP, Zhu J, Guo Z (2021) Tunable positive magnetoresistance of magnetic polyaniline nanocomposites. Adv Compos Hybrid Ma 4:534–542. https://doi.org/10.1007/s42114-021-00242-z
28. Shao Y, Bai H, Wang H, Fei G, Li L, Zhu Y (2021) Magnetically sensitive and high template affinity surface imprinted polymer prepared using porous TiO_2-coated magnetite-silica nanoparticles for efficient removal of tetrabromobisphenol A from polluted water. Adv Compos Hybrid Ma. https://doi.org/10.1007/s42114-021-00361-7
29. Dwivedi M (2018) Exopolysaccharide (EPS) producing isolates from sugarcane field soil and antibacterial activity of extracted EPSs. Acta Scientific Microbiology 1:06–13. https://doi.org/10.31080/ASMI.2018.01.0032
30. Felz S, Vermeulen P, Loosdrecht MC, Lin YM (2019) Chemical characterization methods for the analysis of structural extracellular polymeric substances (EPS). Water Res 157:201–208. https://doi.org/10.1016/j.watres.2019.03.068
31. Kang E, Ting Y, Neoh K, Tan K (1995) Electroless recovery of precious metals from acid solutions by N-containing electroactive polymers. Synthetic Met 69:477–478. https://doi.org/10.1016/0379-6779(94)02533-5
32. Neoh KG, Pun MY, Kang ET, Tan KL (1995) Polyaniline treated with organic acids: doping characteristics and stability. Synthetic Met 73:209–215. https://doi.org/10.1016/0379-6779(95)80018-2
33. Chiang JC, MacDiarmid AG (1986) 'Polyaniline': protonic acid doping of the emeraldine form to the metallic regime. Synthetic Met 13:193–205. https://doi.org/10.1016/0379-6779(86)90070-6
34. Kassahun K et al (2001) Studies on the metabolism of troglitazone to reactive intermediates in vitro and in vivo. Evidence for novel biotransformation pathways involving quinone methide formation and thiazolidinedione ring scission. Chem Res Toxicol 14:62–70. https://doi.org/10.1021/tx000180q
35. Wei Y, Luo W, Zhuang Z, Dai B, Ding J, Li T, Ma M, Yin X, Ma Y (2021) Fabrication of ternary MXene/MnO_2/polyaniline nanostructure with good electrochemical performances. Adv Compos Hybrid Ma 4:1082–1091. https://doi.org/10.1007/s42114-021-00323-z
36. Arasi AY, Jeyakumari JJL, Sundaresan B, Dhanalakshmi V, Anbarasan R (2009) The structural properties of poly (aniline)—analysis via FTIR spectroscopy. Spectrochim Acta A 74:1229–1234. https://doi.org/10.1016/j.saa.2009.09.042
37. Trchová M, Šeděnková I, Tobolková E, Stejskal J (2004) FTIR spectroscopic and conductivity study of the thermal degradation of polyaniline films. Polym Degrad Stabil 86: 179–185. https://doi.org/10.1016/j.polymdegradstab.2004.04.011
38. Du J et al (2020) Boosting the utilization and electrochemical performances of polyaniline by forming a binder-free nanoscale coaxially coated polyaniline/carbon nanotube/carbon fiber paper

hierarchical 3D microstructure composite as a supercapacitor electrode. ACS Omega 5:22119–22130. https://doi.org/10.1021/acsomega.0c02151
39. Mostafaei A, Zolriasatein A (2012) Synthesis and characterization of conducting polyaniline nanocomposites containing ZnO nanorods. Prog Nat Sci Mater 22:273–280. https://doi.org/10.1016/j.pnsc.2012.07.002
40. Gupta P, Dillon AC, Bracker AS, George SM (1991) FTIR studies of H_2O and D_2O decomposition on porous silicon surfaces. Surf Sci Lett 245:360–372. https://doi.org/10.1016/0039-6028(91)90038-T
41. Zhuang Z, Wang W, Wei Y, Li T, Ma M, Ma Y (2021) Preparation of polyaniline nanorods/manganese dioxide nanoflowers core/shell nanostructure and investigation of electrochemical performances. Adv Compos Hybrid Ma 4:938–945. https://doi.org/10.1007/s42114-021-00225-0
42. Nicolet Y, Lacey AL, Vernède X, Fernandez VM, Hatchikian EC, Fontecilla Camps JC (2001) Crystallographic and FTIR spectroscopic evidence of changes in Fe coordination upon reduction of the active site of the Fe-only hydrogenase from *Desulfovibrio desulfuricans*. J Am Chem Soc 123:1596–1601. https://doi.org/10.1021/ja0020963
43. Liu S, Yu B, Wang S, Shen Y, Cong H (2020) Preparation, surface functionalization and application of Fe_3O_4 magnetic nanoparticles. Adv Colloid Interface Sci 281:102165. https://doi.org/10.1016/j.cis.2020.102165
44. Liu B, Wang D, Yu G, Meng X (2013) Adsorption of heavy metal ions, dyes and proteins by chitosan composites and derivatives - a review. J Ocean Univ China 12:500–508. https://doi.org/10.1007/s11802-013-2113-0
45. Yahyaei M, Mehrnejad F, Naderi MH, Rezayan AH (2018) Protein adsorption onto polysaccharides: comparison of chitosan and chitin polymers. Carbohydr Polyme 191:191–197. https://doi.org/10.1016/j.carbpol.2018.03.034
46. Liu B, Wang D, Yu G, Meng X (2013) Adsorption of heavy metal ions, dyes and proteins by chitosan composites and derivatives - a review. J Ocean Univ China 12:500–508. https://doi.org/10.1007/s11802-013-2113-0
47. Huang W, He H, Dong B, Chu H, Xu G, Yan Z (2015) Effects of macro-porous anion exchange and coagulation treatment on organic removal and membrane fouling reduction in water treatment. Desalination 355:204–216. https://doi.org/10.1016/j.desal.2014.10.045
48. Feng Z, Shao Z, Yao J, Huang Y, Chen X (2009) Protein adsorption and separation with chitosan-based amphoteric membranes. Polymer 50:1257–1263. https://doi.org/10.1016/j.polymer.2008.12.046
49. Shi Y, Liu T, Han Y, Zhu X, Zhao X, Ma X, Jiang D, Zhang Q (2017) An efficient method for decoloration of polysaccharides from the sprouts of *Toona sinensis* (A. Juss.) Roem by anion exchange macroporous resins. Food chem 217:461–468. https://doi.org/10.1016/j.foodchem.2016.08.079
50. Yang R, Meng D, Song Y, Li J, Zhang Y, Hu X, Ni Y, Li Q (2012) Simultaneous decoloration and deproteinization of crude polysaccharide from pumpkin residues by cross-linked polystyrene macroporous resin. J Agric Food chem 60:8450–8456. https://doi.org/10.1021/jf3031315
51. Yang X, Yi H, Tang X, Zhao S, Yang Z, Ma Y, Feng T, Cui X (2018) Behaviors and kinetics of toluene adsorption-desorption on activated carbons with varying pore structure. J Environ Sci 67:104–114. https://doi.org/10.1016/j.jes.2017.06.032
52. Yang W, Yu Z, Pan B, Lv L, Zhang W (2015) Simultaneous organic/inorganic removal from water using a new nanocomposite adsorbent: a case study of p-nitrophenol and phosphate. Chem Eng J 268:399–407. https://doi.org/10.1016/j.cej.2015.01.051
53. Craik AD, Leibovich S (1976) A rational model for Langmuir circulations. J Fluid Mech 73:401–426. https://doi.org/10.1017/S0022112076001420
54. Dragan ES, Humelnicu D, Dinu MV, Olariu RI (2017) Kinetics, equilibrium modeling, and thermodynamics on removal of Cr (VI) ions from aqueous solution using novel composites with strong base anion exchanger microspheres embedded into chitosan/poly (vinyl amine) cryogels. Chem Eng J 330:675–691. https://doi.org/10.1016/j.cej.2017.08.004
55. Meng F, Zhou Z, Ni BJ, Zheng X, Huang G, Jia X, Li S, Xiong Y, Kraume M (2011) Characterization of the size-fractionated biomacromolecules: tracking their role and fate in a membrane bioreactor. Water Res 45:4661–4671. https://doi.org/10.1016/j.watres.2011.06.026